Energetics and dynamics for NO and CO dissociation on Cu(100) and Cu(111)

Please check the document version of this publication:

• A submitted manuscript is the version of the article upon submission and before peer-review. There can be important differences between the submitted version and the official published version of record. People interested in the research are advised to contact the author for the final version of the publication, or visit the DOI to the publisher's website.
• The final author version and the galley proof are versions of the publication after peer review.
• The final published version features the final layout of the paper including the volume, issue and page numbers.

[Link to publication](#)

Energetics and Dynamics for NO and CO Dissociation on Cu(100) and Cu(111)

M. A. van Daelen,*,†,§ Y. S. Li,‡ J. M. Newsam,† and R. A. van Santen§

Biosym/MSI, 9685 Scranton Road, San Diego, California 92121-2777, AT&T Bell Laboratories, 67 Whippany Road, Whippany, New Jersey 07981, and Laboratory for Inorganic Chemistry and Catalysis, Eindhoven University of Technology, P.O. Box 513, 5600 MB Eindhoven, The Netherlands

The dissociation of NO and CO has been studied on cluster models representing the copper(100) and -(111) single-crystal faces using density functional quantum calculations. For each surface, several possible reaction paths are proposed, for which we fully optimized the reactant, product, and transition states at the local density level (LDA). Nonlocal density functional calculations (NLDA) were then performed on these optimized geometries. The clusters we used, varying in size between 13 and 31 atoms, produced dissociation barriers and energies that were reasonably well converged with cluster size. Classical transition-state theory was used to calculate the rates of dissociation and recombination on the basis of computed frequencies of the predicted transition state and the reactant and product states. The transition states for NO and CO dissociation on all surfaces can be described as "tight" transition states corresponding to preexponentials for dissociation in the range $10^{10}-10^{13}$ s^{-1}. The dissociation barrier for NO is significantly lower than that for CO. In addition, the more open Cu(100) surface is more reactive toward dissociation than the close-packed Cu(111) surface. Nonlocal corrections to the LDA functional were found to have a small effect on dissociation barrier height, but the effect was found to be more profound on the recombination barrier and overall dissociation energies.

I. Introduction

The decomposition of NO$_x$ species in traditional automotive catalytic converters by means of catalytic reduction has been the subject of many experimental and theoretical studies. Practical catalysts incorporate Rh and Pt, but the activity of Ru, Ni, and Cu has also been examined.[1−5] For an exhaust catalyst to be effective, it needs to facilitate the decomposition of NO$_x$ species to atoms, which can then recombine to N$_2$. At the same time, it should catalyze a nondissociative adsorption of CO followed by oxidation of adsorbed CO to CO$_2$. The dissociation of NO is often the rate-limiting reaction step in this process.[1,6,7] The activity of Rh and Pt can be explained because of the low barrier toward NO dissociation, while the CO barriers are high enough to preclude dissociation. The dissociation of CO itself is analogous to the NO dissociation and is of importance, among others, in the production of hydrocarbons from carbon monoxide and hydrogen, which are components of synthesis gas.[8]

Progressively more stringent auto emission standards have necessitated the development of a new catalyst for NO reduction, most particularly, a catalyst that performs efficiently in the lean burn regime. Traditional catalysts, although sufficiently active in hydrocarbon (HC) and CO oxidation, deliver poor DeNO$_x$ performance at these leaner levels. Converters with different catalysts for the oxidation and reduction stages are therefore being pursued. A promising candidate consists of zeolite-supported copper clusters. In particular, the Cu/ZSM-5 system has shown extreme large activity toward NO reduction, orders of magnitude larger than systems based on other zeolites.[9] However, the mechanism of both their catalytic action and of their deactivation in the presence of water vapor is unknown.

Also, the thermal stability of the zeolite framework is insufficient to make the application of this system commercially viable at present.

Additional research aimed at elucidating the mechanism and understanding how structural properties might affect the catalytic activity is needed for both zeolite- and metal-based catalysts. The first category is cumbersome to deal with computationally since little is known about the structure of the active sites in the zeolite. Metal catalysts are at this point more attractive since it is relatively well understood what the mechanism is for dissociation and what the structural properties are of the active centers. With the emerging accurate and efficient quantum methods, this is a very attractive area to explore. In a span of about 5 years, the typical size of a metallic system that could be handled at the *ab initio* level has increased from a few (<5) to some 30−50 atoms at present. This allows the study of model systems of a size that is catalytically relevant, as was already shown for homogeneous catalytic systems by Ziegler.[10]

Predicting the transition state and, hence, the energy barriers for the dissociation reactions on these metals is primary to determine their value as NO reduction catalysts. Studying the dynamical properties of these transition states allows, in addition, access to the rate for the reaction using transition-state theory. The dissociation properties are closely related to the d-electronic structure of the metal, and therefore, elements neighboring those that are currently applied in the periodic system (Pt, Rh) are also principle candidates for effectively catalyzing the NO reduction. The present study concerned Cu, which is relatively easy to handle computationally since it is not a pure transition metal. In an undergoing study, we are addressing other metals like Ni.[11]

There is ample experimental data available on the adsorption properties of NO and CO on copper surfaces. CO is known to adsorb linearly by the C atom in low coordination sites on copper(111) and -(100) surfaces, but the energy difference

between different coordination sites is expected to be small.[12] This is supported by experiments showing that depending on coverage, a variety of sites are occupied by CO.[13] Molecular NO is usually adsorbed in a linear or bent configuration on top or bridge sites. However, dissociative adsorption is observed even at low temperatures.[14,15] Ground-state vibrational frequencies have been measured using infrared spectroscopy (IRS) and electron energy loss (EELS) techniques, providing information about frequencies associated with the metal−adsorbate bond-stretching modes as well as the internal modes of the adsorbate. Also, bending modes of the adsorbate can be detected with EELS; however, the interpretation of intensities is difficult because of competition in this low wavenumber range with atomic adsorbate modes and the surface phonon background.

The majority of the experimental data on reaction barriers and the dynamics of the dissociation process are of a qualitative nature rather than quantitative. Balkenende *et al.*[16,17] reported a higher activity for NO dissociation on the more open Cu-(100) and Cu(110) surfaces than on the close-packed Cu(111) surface. In addition, they found the dissociation barrier for NO to be much lower than for CO; NO tends to adsorb dissociatively, while the barrier for CO precludes dissociative adsorption. Also for Pt, the (100) surface was found to be more active in inducing the dissociation of NO compared to the (111) surface.[3] Brodén *et al.*[18] made a comparison of available data for chemisorption of diatomic molecules and related the probability of the molecule to dissociate on a metal surface to the position of the metal in the periodic system. The height of the activation barrier decreases as one goes to the left in the periodic table. The transition from dissociative to associative adsorption is different for CO and NO (as NO dissociation barriers are usually lower) and is also a function of the surface geometry. Experimental preexponential factors measured on various metal surfaces lie within 1×10^9 and 1×10^{12} s^{-1} for diatomic dissociation reactions.[19] These studies showed that the dissociation proceeds via a mechanism requiring a vacant nearest-neighbor site for the adsorbed diatomic.

There are a number of theoretical studies on the energetics of CO and NO adsorption on copper surfaces. Post and Baerends[20] studied CO adsorption on small Cu clusters (1−7 atoms) using density functional theory and found reasonable agreement with experiment for bond distances and vibrational frequencies even for small CO/Cu$_n$ systems. The adsorption energies, on the other hand, showed a strong dependence with cluster size, and for most clusters, they found hollow adsorption sites to be preferred over top sites. These results are due to the high degree of coordinative unsaturation of the cluster atoms compared to the bulk atoms. Typically, even a 10-atom cluster has only 1 atom coordinated to 9 neighbors, similarly as in the bulk Cu(111) surface. In a recent study on CO adsorption on Cu(100), strong oscillations were reported for the CO binding energy on clusters up to 37 atoms.[21] These oscillations are found to be caused by very small changes in the density of states of clusters when the cluster size changes. However, the clusters as used in their study consist predominantly of only a monolayer of metal atoms. Hence, the metal atom binding to the adsorbate is missing all neighbors in the second layer, resulting in unrealistic reactivity of this central atom. Bauschlicher has shown clusters with less than 14 atoms to be definitely too small, but clusters of 14−38 atoms to be possibly accurate. Siegbahn found a similar result; H on Ni$_{19}$(12,7) gives 27.5 kcal/mol and H on Ni$_{40}$(21,13,6) gives 46.5 kcal/mol, to be compared to experimental 63 kcal/mol. Siegbahn also showed that oscillations in adsorption energies as a function of cluster size could be diminished by adsorbing on geometrically optimized clus-

ters[30] or by exciting the cluster to a proper bonding state, reasoning that such a state would always be present at the extended surface.[31] The first procedure is valuable for studying cluster properties, but when bulk surfaces are studied, the optimized cluster geometry will usually distort from the bulk geometry, making them less appropriate to model an extended surface. Preparing the cluster for bonding is less practical for studying surface reactions since different stationary points on the reaction path might need different bond preparation for the cluster. We will address the issue of cluster size convergence in the present study, and we present clusters that give reasonable adsorption energies and good dissociation energetics.

Early studies on dissociation reactions on small clusters modeling metal surfaces involved hydrogen, and these delivered very valuable insights in the basic chemistry of molecules interacting with surfaces, notwithstanding the limited size of the clusters involved in these studies.[24,25] More recently, Yang and Whitten[26] used a many-electron embedding theory to calculate barriers for H$_2$ dissociation on a Ni(100) surface. They obtained accurate bond energies, vibrational frequencies, and activation barriers for dissociation, and determined the site preference for H adsorption.

Earlier we presented a quantum chemical analysis of CO dissociation on different surfaces of Rh based on the ASED molecular orbital method, an adapted version of the semiempirical extended Hückel method.[27] This study permitted a qualitative description of the transition state for the surface dissociation and allowed a comparison of the activation barriers for dissociation along a number of different reaction paths. Dissociation follows a clear pattern. Starting from a position parallel to the surface normal, the oxygen atom tilts toward the metal surface and the C−O bond stretches. During this stretch, crossing of the C−O bond over a surface metal atom is favored. This maximizes the overlap between one of the $2\pi^*$ orbitals of the molecule and appropriate d orbitals on the metal atom. After dissociation, the carbon and the oxygen atom share the least number of surface metal atoms to minimize the repulsive interaction between the atomic species.[28] The study also indicated significant larger activity toward CO dissociation for a Rh(100) surface than for a Rh(111) surface. Van Langeveld *et al.*[29] performed extended Hückel calculations on CO dissociation on Ni(111) and found a dissociation barrier almost equal to the CO adsorption energy. A first attempt to model dissociation barriers for CO on copper surfaces was reported by Siegbahn, who performed MCPF calculations on CO adsorbed on a 12-atom cluster model of a Cu(100) surface. A transition state for CO dissociation over a metal bridge site was approximated, resulting in a barrier of the order of 11 kcal/mol. While each of these studies provided useful information toward the qualitative understanding of metal-catalyzed bond breaking in diatomics, the absence of a complete transition-state optimization and limitations in the methods used precluded any quantitative energetics.

Recently, we have demonstrated the applicability of the density functional approach to predict transition states. Based on these results, the rate constant for the dissociative adsorption of methane on Ni clusters was computed,[32−34] as well as the rate constant for hydrogen exchange and dehydrogenation of methane on a zeolitic acid site.[35] The transition-state barrier energies computed on transition-metal clusters depend on cluster size, but especially for cuboohedral transition-metal clusters of 13 atoms, predicted values were close to experiment.[34] In the present study, we have applied the density functional approach to the dissociation of diatomics on single-crystal copper surfaces represented by cluster models. The question of cluster size

NO and CO Dissociation on Cu(100) and Cu(111)

J. Phys. Chem., Vol. 100, No. 6, 1996 **2281**

dependence is addressed. We fully optimized the transition states with respect to all degrees of freedom for the adsorbate in the plane of symmetry. In addition to our recently reported study,[36] we now also calculated the energetics by applying a Becke−Perdew nonlocal correction to repair the error in the exchange−correlation terms. Nonlocal corrections are routinely applied nowadays because they result in more accurate binding energies. In this study, we will investigate the importance of these corrections. The clusters we are using are also substantially larger than those that were used in the previous study to minimize finite cluster size effects. Having obtained one well-defined reaction path, we applied transition-state theory to calculate the reaction rate constants for the dissociation and recombination along the particular path. We used a full vibrational analysis for all degrees of freedom of the adsorbate to calculate the partition functions for reactant, product, and transition states. We use this to estimate the entropy factor, which together with the activation energy defines the reaction rate constant.

In section II, we discuss the methodology of the calculations and the theory used to calculate the reaction rate constants for a surface reaction. Section III deals with the properties of the reactant and product states on the various dissociation paths; this includes adsorbate geometries, vibrational frequencies, and adsorption energies. We also discuss the transition states and the energy barriers for dissociation and recombination and present a normal mode analysis for the stationary points on the reaction paths and the calculated preexponential factors. Our conclusions are summarized in section IV.

II. Methodology and Theoretical Background

A. Computational Details. The computations reported in this work were performed using the density functional program DMol, which is an implementation of the Kohn−Sham equations.[37,38] We used numerical basis sets of double-ζ quality and polarization functions for Cu. The Von Barth−Hedin parameterization[39] of the results of Ceperley and Alder's homogeneous electron gas calculations[40] was used to describe the exchange−correlation energy. Becke−Perdew nonlocal gradient corrections[41,42] were applied self-consistently to the optimized geometries of the stationary points on the reaction paths. To improve the scf convergence for some systems, we allowed charge smearing for orbitals within 0.005 Ha of the Fermi level.

The energetics and dynamics of the dissociation of nitric oxide and carbon monoxide were investigated on clusters varying in size from 8 to 31 atoms that were clipped from the extended surface with a lattice constant of 3.61 Å, in order to model the Cu(111) and Cu(100) surfaces. These cluster models give a reasonable geometrical representation of an extended surface since these surfaces are known to reconstruct only to a small extent.[43,44] The sizes of some of the clusters are such that computed adsorption energies are still sensitive to electronic edge effects. The larger clusters were used to investigate the importance of these effects.

The reaction paths that we studied (Figure 1) were similar to the lowest energy paths for CO dissociation on Rh from a previous publication in our group.[27] For each Cu surface cluster, we studied two essentially different pathways, one in which the diatomic is bending over a bridge of two metal atoms (a, c), the other where it bends over a top site of the metal surface (b, d). We used 10- and 31-atom clusters to model the Cu(111) surface and 8-, 13-, 14-, and 28-atom clusters to model the Cu(100) surface. The 31- and 28-atom clusters consist of all first nearest neighbors of the metal atoms coordinating to the
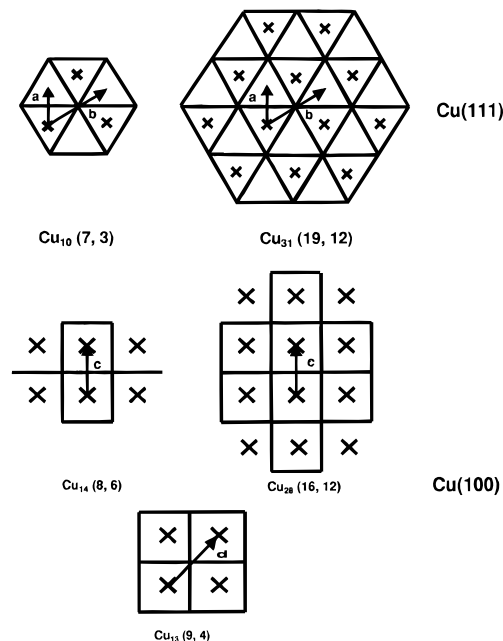

Figure 1. Pathways for CO and NO dissociation on cluster models of Cu(111) and Cu(100) surfaces. Drawn lines connect Cu atoms in the first layer. Crosses depict Cu atoms in the second layer. The pathways for dissociation are indicated by arrows which connect the site where the molecule is adsorbed in the reactant state and the site where the oxygen atom is positioned after dissociation. The molecule tilts in the direction of the arrow.
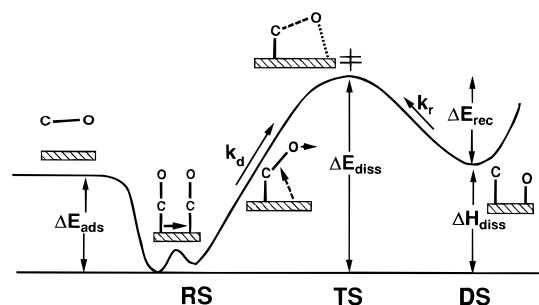

Figure 2. Schematic energy profile for the surface dissociation. The stationary points on the reaction path are the reactant state (RS), the product or dissociated state (DS), and the transition state (TS). The diffusion step is necessary for the adsorbate to migrate to a preferred site for dissociation (see text). The metal surface activates the intermolecular bond and facilitates the bond breaking. Energetic parameters of interest are the adsorption energy E_{ads} and the barriers for dissociation (ΔE_{diss}) and recombination (ΔE_{rec}). The kinetics were monitored by means of the preexponential factors for dissociation K_d and recombination K_r.

dissociating diatomic. As is shown in Figure 2, we will refer to the initial state where the diatomic is molecularly adsorbed as the *reactant state* (RS). The final state with the atoms isolated on the surface will be referred to as the *product state* or *dissociated state* (DS). The saddle point connecting the reactant and product valley is the *transition state* (TS). All reaction paths lie in the C_s symmetry plane of the cluster.

The 3- and 4-fold hollow locations, which are the reactant state geometries, are known to be less stable than the top sites for both CO and NO. So the molecule needs to move to a hollow site to be in a preferred position for dissociation. Since the difference in energy between the top and 3- or 4-fold hollow sites is small,[12] the top−hollow site interchange will not be rate limiting.

The approximate location of the transition state was obtained by taking steps along the reaction path and optimizing the height

of the oxygen atom while keeping the carbon atom fixed at the height of adsorbed C. This results in a good estimate for the location of the transition state that can then be used for further geometry refinement. We used a "normal mode following" algorithm developed and implemented by Baker[45] to optimize all the degrees of freedom for the adsorbing species in the plane of symmetry. Typically, 8−10 iterations were needed to locate the transition state. Speed up of this procedure was achieved by sharing the Hessian matrices between cluster−adsorbate systems of varying sizes. All calculations were performed on SGI Indigo 2 workstations and took between 1 h for the smaller clusters and up to 48 h for the largest systems to complete.

B. Transition-State Theory. A diatomic molecule adsorbed on a surface will usually require a vacant nearest-neighbor site to dissociate. For instance, for NO dissociation,

$$NO^* + * \rightarrow N^* + O^* \tag{1}$$
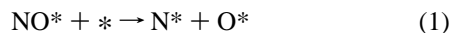
where an asterisk denotes an adsorbed species or a vacant site. Moving on the reaction path from the reactant state to the dissociated state, the molecule will traverse through a transition state. We will use classical transition-state theory[46] to compute rate constants from the local properties of these stationary points on the potential energy surface. For the surface dissociation and recombination, the rate constants k_{dis} and k_{rec} at temperature T are given by[46,47]

$$k_{dis} = \frac{k_B T}{h} \frac{Q'^{TS}}{Q'^{RS}} e^{-E_0/(k_B T)} \tag{2}$$

and

$$k_{rec} = \frac{k_B T}{h} \frac{Q'^{TS}}{Q'^{DS}} e^{-E_0/(k_B T)} \tag{3}$$

with

$$Q' = Q\left(\prod_i e^{+(1/2)[(h\nu_i)/(k_B T)]}\right) \tag{4}$$

where k_B is Boltzmann's constant, h is Planck's constant, and E_0 is the difference in energy per mole between the activated complex and the reactants, not corrected for the zero-point energy vibrations. Q'^{RS}, Q'^{TS}, and Q'^{DS} are the partition functions at the reactant state, the transition state, and the dissociated state, respectively. The partition functions can approximately be factorized into translational, rotational, and vibrational factors. In the present study, the solid surface is assumed to be rigid; therefore, the partition functions for the surface are equal to unity and do not appear in the rate equation. In addition, if for a surface reaction the adsorbates and the activated complex are localized on the surface, there is no rotational or translational motion but only vibrational modes. For the vibrational partition function Q_{vib}, we have used the decomposition in normal modes ν_i using the harmonic approximation, yielding

$$Q_{vib} = \prod_i^{modes} \frac{1}{1 - e^{-(h\nu_i)/(k_B T)}} \tag{5}$$

where Q_{vib} is the vibrational partition function for the $3N$ modes of the adsorbate ($3N - 1$ for the transition state).
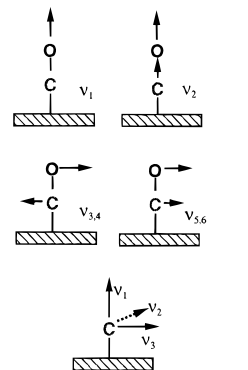

Figure 3. Normal modes for a diatomic (a) and monoatomic (b) surface adsorbate. Surface atoms are fixed and have no vibrational freedom.

The normal modes for the RS and DS are schematically depicted in Figure 3. For the reactant state, a normal mode analysis yields a high-frequency CO/NO stretch (ν_1), a Me−CO/NO stretch (ν_2), two degenerated hindered rotations (ν_3,ν_4), and two degenerated hindered translations (ν_5,ν_6). The degeneracy is a consequence of the C_{3v} and C_{4v} point groups of the adsorption sites, but when asymmetric clusters are used, the degeneracy will be lifted. The CO and NO stretch frequencies are usually 100−300 cm^{-1} below the equilibrium gas-phase stretching frequencies (2170 cm^{-1} for CO and 1820 cm^{-1} for NO[48]) depending on the adsorption geometry. The other modes are all expected to be below 800 cm^{-1}. Inspecting the expression for the vibrational partition functions tells us that only modes lower than 200 cm^{-1} will result in a partition function substantially larger than unity. Hindered translations typically have a very low frequency, sometimes below 100 cm^{-1}, and have the highest weight in the calculation of the partition functions. Alternatively, the zero-point energies contribution to the activation energy will mainly come from the high-frequency modes. The dissociated state is characterized by six frequencies that are roughly vibrations in x, y, and z for C/N and O, with possible coupling between these modes. For the transition state, we expect one imaginary frequency corresponding to the reaction coordinate and five real modes of rather complex nature.

The vibrational modes for the adsorbate were calculated harmonically by diagonalizing the second-derivative matrix. Second derivatives were computed by taking finite differences of analytical first derivatives. The gradients were calculated for the equilibrium geometry and for the geometries with atoms displaced along the 6 degrees of freedom. The displacements were typically of the order of 0.01 bohr, but in cases of very flat energy wells, displacements up to 0.03 bohr were used. The reaction rates were calculated at temperatures in the range 300−1000 K and fit to an Arrhenius equation to obtain values for the preexponential factor and the experimentally measurable activation energy.

III. Results and Discussion

The results are discussed in terms of (A) the energetic and geometric properties of CO adsorption as a function of cluster size, (B) the properties of the reactant and product states for CO and NO dissociation, (C) the transition states and the resulting barriers for CO and NO dissociation and recombination, and (D) the normal modes for the adsorbates and preexponential factors for the reactions. Subsequent energetic analyses are based primarily on the energies that include Becke−Perdew nonlocal corrections. A comparison with the local results will be made.
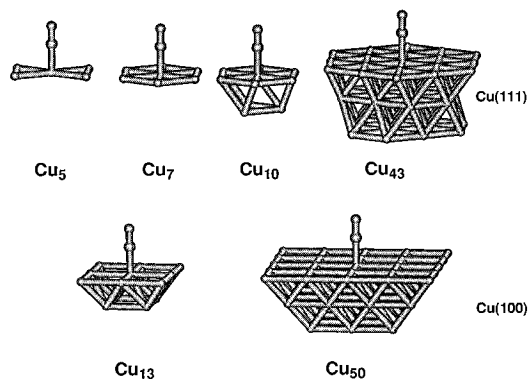
Figure 4. Clusters used to study size dependence of adsorption properties. The Cu_5, Cu_7, Cu_{10}, and Cu_{43} clusters represent the Cu-(111) surface, and the Cu_{13} and Cu_{50} clusters represent Cu(100).

TABLE 1: Energetic (in kcal/mol), Structural (in Å), and Vibrational (in cm^{-1}) Properties for CO Adsorbed Atop Clusters Modeling Cu(111) and Cu(100) Surfaces

cluster	surface	E_{ads}^{LDA}	E_{ads}^{NLDA}	h^b	d_{C-O}	ν_{C-O}	ν_{Cu-C}
Cu_5	(111)	−26.0	−9.1	1.849	1.160	2028	388
Cu_7		−24.4	−6.9	1.874	1.157	2029	318
Cu_{10}		−19.5	−1.4	1.853	1.155	2044	336
Cu_{43}		−21.6	−4.3	1.908	1.162	1993	339
exptl		−12.0[13]		1.90[13]	1.15[13]	2079[13]	
Cu_{13}	(100)	−25.8	−6.7	1.795	1.153	2077	374
Cu_{50}		−34.4	−15.6	1.805	1.159	2007	398
exptl		−16.7[12]		1.90[61]	1.16[61]	2064[12]/2090[62]	340[62]

^{a} The nonlocal energies are calculated for LDA optimized geometries. The structural and vibrational numbers were calculated at the local level. Clusters are shown in Figure 4. ^{b} h is the distance between the carbon atom and the top plane of the Cu atoms.

A. Cluster Size Dependence: CO Top Adsorption. To estimate the dependence of the energetics, the geometries, and the vibrational frequencies on cluster size, we studied in more detail the molecular adsorption of CO in a top site on clusters representing Cu(111) and Cu(100) surfaces. Characteristics of CO adsorption on Cu_n clusters ($n = 5, 7, 10, 43; 13, 50$) modeling the (111) and (100) surfaces (shown in Figure 4) are summarized in Table 1 and compared with experimental data. For these clusters, we could take advantage of either C_{2v}, C_{3v}, and C_{4v} point-group symmetry in the calculations. The properties that have been studied for top adsorption are the equilibrium height of CO above the surface (h) the CO internuclear distance (d_{C-O}), the CO stretch frequency (ν_{C-O}), and the frequency of the CO vibration against the surface (ν_{Cu-C}). The molecular adsorption energies are calculated by subtracting the binding energy for the bare cluster and the binding energy for the free molecule from the binding energy of the combined system:

$$E_{ads} = E_b(Cu_nCO) - E_b(Cu_n) - E_b(CO) \quad (6)$$

For NO, we will later use an analogous expression. We used calculated local (and nonlocal) dissociation energies in (kcal/mol) of −288.0 (−266.5) for gas-phase CO and −185.0 (−162.3) for gas-phase NO.

The calculated values for the adsorption height, the C−O bond length, and the vibrational frequencies are within reasonable limits of the experimental values and in agreement with the calculations of Post and Baerends.[20] The change in C−O equilibrium distance and in C−O vibrational frequency upon adsorption, corresponding to an elongation and weakening of the bond, shows fairly rapid convergence with increasing cluster size. These properties can therefore be called "localized", since they appear to be converged even without the central metal atom

TABLE 2: Energetic (in kcal/mol) and Structural (in Å) Properties for the Reactant States for CO and NO Dissociation

adsorbate	path	cluster	surface	E_{ads}^{LDA}	E_{ads}^{NLDA}	h^a	d_{C-O}
CO	a, b	Cu_{10}	(111)	−24.8	0.3	1.34	1.19
		Cu_{31}		−37.7	−11.5	1.33	1.19
	c	Cu_8	(100)	−39.8	−13.9	1.15	1.20
		Cu_{14}		−35.6	−9.1	1.11	1.21
		Cu_{28}		−31.9	−4.6	1.09	1.21
	d	Cu_{13}		−36.4	−9.0	1.06	1.21

adsorbate	path	cluster	surface	E_{abs}^{LDA}	E_{ads}^{NLDA}	h^a	d_{N-O}
NO	a, b	Cu_{10}	(111)	−44.5	−18.0	1.28	1.23
		Cu_{31}		−48.4	−22.1	1.30	1.22
	c	Cu_8	(100)	−52.5	−24.6	1.03	1.24
		Cu_{14}		−51.9	−26.2	1.13	1.24
		Cu_{28}		−45.6	−16.9	0.98	1.26
	d	Cu_{13}		−47.2	−19.2	1.02	1.25

^{a} h is the distance between either the carbon or the nitrogen atom and the top plane of the Cu atoms.

being fully coordinated. The adsorption energies, on the other hand, are not well converged. In fact, on Cu(111), the absolute value of the adsorption energy decreases until the first nearest-neighbor shell of the metal atom is completed due to large energetic changes in the clusters themselves upon adsorption.[49] Adding second nearest neighbors (from Cu_{10} to Cu_{43}) affects the binding energy only slightly. This behavior is consistent with Shustorovich's bond order conservation principle,[28] where each atom is thought to have a certain amount of "bonding power" shared between all of its neighbors. When the first neighbor shell is incomplete, there will be a greater availability of electrons for bond formation to adsorbed species than in the bulk surface. Hence, the adsorbates are usually overbound when the atom(s) coordinating to the adsorbate has unsaturated valencies. However, the errors made in the reactant, product, and transition states will approximately cancel, resulting in reasonably accurate values for reaction energetics and barriers.

The local adsorption energies for Cu(111) appear to be smaller than the experimental number, which is expected given that LDA typically overestimates bond energies. The nonlocal corrections essentially overcorrect these numbers, and the problem of how to achieve high accuracy on chemisorptive bond strengths remains. For the Cu(100) surface, we see a large increase in the adsorption energy when adding the second shell of the metal atoms. This indicates that the Cu_{13} cluster is still too small to represent the Cu(100) top adsorption site, which was also concluded by Bauschlicher.[22] For Cu(100), the Cu_{50} cluster gives a nonlocal value of −15.6 kcal/mol, which is in good agreement with experiment.

As we present the properties for hollow site adsorption in the next paragraph, we see a preference for hollow over top adsorption, which contradicts experiment.[12] This problem is still present, although less severe, after applying nonlocal corrections. Cluster size effects or coverage dependence may therefore still be of importance. Very promising results were reported using slab calculations for CO monolayer adsorption on Cu(100).[21,23] However, this matter is beyond the scope of this study since our prime interest is the dissociation reaction rather than chemisorption.

B. Reactant and Product States for the Surface Dissociation. On the proposed reaction paths as shown in Figure 1, we studied the adsorption properties for the reactant and product states in order to calculate the energetics for the dissociation reaction. The adsorption properties for the reactant states on the various reaction paths, i.e., NO and CO adsorbed in 3- and 4-fold hollow sites, are given in Table 2. We optimized the

TABLE 3: Energetic (in kcal/mol) and Structural (in Å) Properties for the Dissociated States for CO and NO Dissociation[a]

adspecies	path	cluster	opt coords	E_{ads}^{LDA}	E_{ads}^{NLDA}	h_C[b]	h_O[b]	d_{C-O}[c]
C + O	a	Cu_{10}	xz	no local min				
	b	Cu_{10}	z	+41.2	+76.5	1.10	1.16	2.95
		Cu_{31}	z	+37.6	–	1.15	1.15	2.95
			xz	+34.5 (−3.1)	+73.6	1.14	1.14	3.05
	c	Cu_8	z	−4.9	+44.6	0.07	0.75	2.66
		Cu_{14}	z	+13.5	+58.7	0.15	0.88	2.66
		Cu_{28}	z	+11.7	–	0.15	0.84	2.65
			xz	+3.6 (−8.1)	+49.0	0.28	0.98	3.03
	d	Cu_{13}	z	−18.4	–	0.17	0.74	3.66
			xz	−19.4 (−1.0)	+29.9	0.20	0.74	3.75

adspecies	path	cluster	opt coords	E_{ads}^{LDA}	E_{ads}^{NLDA}	h_N[b]	h_O[b]	d_{N-O}[c]
N + O	a	Cu_{10}	xz	no local min				
	b	Cu_{10}	z	−34.9	+0.4	1.08	1.16	2.95
		Cu_{31}	z	−37.4	–	1.10	1.15	2.95
			xz	−38.5 (−1.1)	−3.0	1.11	1.15	3.10
	c	Cu_8	z	−53.2	−3.8	0.10	0.80	2.66
		Cu_{14}	z	−45.4	−3.3	0.38	0.63	2.56
		Cu_{28}	z	−56.7	–	0.57	0.78	2.56
			xz	−63.2 (−6.5)	−21.7	0.56	0.92	2.92
	d	Cu_{13}	z	−77.0	–	0.45	0.78	3.63
			xz	−79.2 (−1.8)	−35.0	0.50	0.76	3.82

[a] Indicated are the coordinates for which the adsorbing atoms are optimized (z or xz). E_{ads}^{LDA} and E_{ads}^{NLDA} are the local and nonlocal total adsorption energies for the coadsorbed atoms. The energy values in parentheses are the energy differences between the z- and xz-optimized geometries. Nonlocal energies were only calculated for the geometries that were used to evaluate the energy barriers (see text). [b] h is the distance between the carbon/nitrogen atom and the top plane of the Cu atoms. [c] The distance between the atoms after dissociation.

height of the adsorbate, while leaving the other coordinates for the adsorbate frozen, in order not to break the local symmetry of the adsorption site. Especially for the smaller clusters, this appeared to be a necessity. Due to the high reactivity of the edge atoms, which is a cluster artifact, the diatomic tends to bend, and in a few cases, the adsorbate actually relaxed to a 2-fold edge position. Fixing the diatomic symmetrically in that site and only optimizing perpendicular degrees of freedom will therefore give the most realistic energies in the absence of a local minimum.

Comparing adsorption for CO in the hollow sites with that for atop adsorption (Table 1) shows stronger bonding in higher coordination sites for the Cu(111) surface. For instance, compare the CO nonlocal binding energy of −4.3 kcal/mol atop the Cu$_{43}$ cluster with that of −11.5 kcal/mol for CO adsorption in the hollow site of the Cu$_{31}$ cluster. However, for Cu(100), the top site is preferred over the hollow site. Adsorption on the top site of Cu$_{50}$ shows a binding energy of −15.6 kcal/mol, whereas the binding energy for the hollow site on Cu$_{31}$ is −4.6 kcal/mol. The LDA results show the same trends. However, especially for hollow site adsorption, oscillations in the binding energy resulting from cluster size effects are large, making it difficult to predict the relative stability of the sites. No experimental data on hollow site adsorption for CO and NO are available, but for CO, it is expected to be close to the top adsorption energy. For that reason, the nonlocal adsorption energies for the largest clusters are very reasonable.

The adsorption properties for the dissociated states are reported in Table 3. The adsorption energies are calculated with respect to the bare cluster and the diatomic in the gas phase, similarly as for the reactant state (eq 6). These energies are a measure of the relative stability of the different product states. We first optimized the adsorbate coordinates perpendicular to the surface (rows z). We subsequently relaxed the coordinate in the plane of symmetry to account for the repulsion between the fragments (rows xz). For some of the smaller clusters, the adsorbate fragments relaxed to an edge position, again due to the coordinative unsaturation of the edge atoms. The energy well for atomic adsorption is apparently very flat in these cases,

causing a relaxation of unphysical nature. Therefore, for the clusters with 8, 10, and 14 atoms, we used the energies for the systems that were only optimized in the direction perpendicular to the surface for calculating the reaction energetics.

The bending of CO and NO over a bridge on Cu(111) (reaction path a) was rejected as a likely reaction path because the dissociated states appeared to be unstable. When relaxing this state, the atomic fragments recombine without barrier because the "isolated" atoms coadsorbed at adjacent 3-fold sites in the DS (across a Cu−Cu bond) are relatively close (1.48 vs 1.15 Å in molecularly adsorbed CO). There is still an attractive interaction between these atoms, which implies that the molecular bond is not broken. This rules out dissociation along this particular path. A similar observation was reported for hydrogen dissociation along an identical pathway on Ni(111).[26]

The binding energies for the reactant and product states allow us to calculate the reaction energy for dissociation, which is defined here as the difference in total binding energies of RS and DS:

$$\Delta H_{diss} = E_b(DS) - E_b(RS) \qquad (7)$$

These total energies are not listed, but the dissociation energy can alternatively be obtained by combining this expression with the expression for the molecular adsorption energy (eq 6), yielding

$$\Delta H_{diss} = E_{ads}(DS) - E_{ads}(RS) \qquad (8)$$

These are reported in Table 4.

Dissociation of CO is endothermic for all reaction paths. The differences in dissociation energies on the various surfaces can be explained from the geometries of the dissociated states. Both the lateral distance between the fragments and the adsorption site coordination are important. For reaction paths b (d_{lat} = 2.95 Å) and d (d_{lat} = 2.65 Å), the atoms are adsorbed at adjacent sites, sharing one surface metal atom, while on reaction path c (d_{lat} = 3.66 Å), they are sharing two metal atoms. On Cu(111), reaction path b has an energy for C + O coadsorption

NO and CO Dissociation on Cu(100) and Cu(111)

J. Phys. Chem., Vol. 100, No. 6, 1996 **2285**

TABLE 4: Dissociation Energies and Activation Barriers for Dissociation and Recombination (in kcal/mol) of CO and NO on the Various Reaction Paths

	path	cluster	surface	ΔH_{diss} LDA	ΔH_{diss} NLDA	$\Delta E^{\ddagger}_{\text{diss}}$ LDA	$\Delta E^{\ddagger}_{\text{diss}}$ NLDA	$\Delta E^{\ddagger}_{\text{rec}}$ LDA	$\Delta E^{\ddagger}_{\text{rec}}$ NLDA
CO	b	Cu_{10}	(111)	+66	+76	97	99	31	23
		Cu_{31}		+72	+85	108	108	36	23
	c	Cu_8	(100)	+35	+58	79	91	44	32
		Cu_{14}		+49	+68	76	88	27	20
		Cu_{28}		+44	+65	74	85	38	31
	d	Cu_{13}		+18	+39	88	93	70	54
NO	b	Cu_{10}	(111)	+10	+18	62	62	52	44
		Cu_{31}		+11	+20	54	54	43	34
	c	Cu_8	(100)	−1	+21	46[a]	54	47	33
		Cu_{14}		+7	+23	39	50	32	27
		Cu_{28}		−11	+3	35	38	46	34
	d	Cu_{13}		−30	−9	41[a]	44	71	54

[a] These barriers are both somewhat larger than in ref 36 because a smaller charge smearing value resulted in a lower energy for the reactant states.

of +74 kcal/mol (Cu_{31}), while on Cu(100), reaction paths c and d have coadsorption energies of +49 kcal/mol (Cu_{28}) and +30 kcal/mol (Cu_{13}), respectively. The first conclusion is that the isolated atoms are bonded stronger in the hollow sites on Cu(100) than in the 3-fold sites on Cu(111), agreeing with the commonly observed tendency for atoms to favor high coordination. Second, since the lateral spacing is significantly larger for the hollow sites on diagonal path d than on bridged path c, there is more repulsion in the dissociated state of the bridged reaction pathway, making the pathway more endothermic (+49 vs +30 kcal/mol). This trend is also manifested in the energy that is released when the adsorbate atoms are allowed to relax in lateral direction z in addition to perpendicular direction x (Table 3). This relaxation energy is −8.1 kcal/mol on reaction path c (Cu_{28}) and only −3.1 and −1.0 kcal/mol on reaction paths b and d (Cu_{31} and Cu_{13}). For NO, we find the same trends of stronger atomic adsorption on Cu(100) than on Cu(111) and stronger repulsion when the atomic fragments are adsorbed at smaller distances.

Besides a distance argument, the high relaxation energy for the Cu_{28} cluster could also be explained in terms of screening of the fragment interactions by a metal atom. This is more important when the fragments are adsorbed on adjacent sites sharing one surface atom than when they are adsorbed across a Cu−Cu bridge. The stability of the dissociated state is not only important in the overall reaction energetics, but a stable end configuration also lowers the activation barrier,[27] as we will show later.

C. Transition States for Dissociation. Except for reaction path a, where we don't expect a transition state, we were able to locate the transition states for all other proposed pathways (Figure 5). The activation barriers for the dissociation and recombination reactions are derived from the energies for these transition states

$$\Delta E^{\ddagger}_{\text{diss}} = E_b(TS) - E_b(RS) \qquad (9)$$

and

$$\Delta E^{\ddagger}_{\text{rec}} = E_b(TS) - E_b(DS) \qquad (10)$$

These energies are listed in Table 4.

We first consider the cluster size dependence of activation barriers and dissociation energies by comparing identical pathways c on clusters of increasing size. The differences between Cu_{10} and Cu_{31} for the barriers and reaction energies
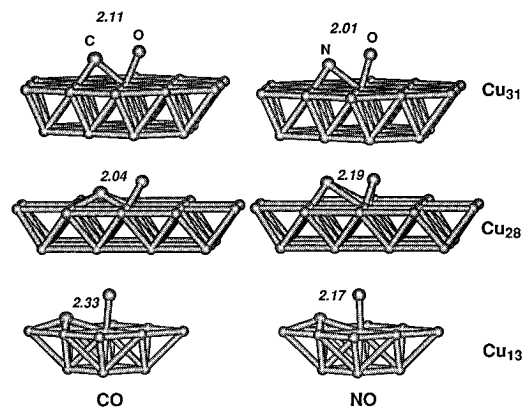

Figure 5. Optimized transition-state geometries for CO (left) and NO dissociation (right) on Cu_{31} (Cu(111)) and Cu_{28} and Cu_{13} (Cu(100)) cluster models, corresponding to reaction paths b, c, and d from Figure 1. CO and NO distances are indicated in angstroms.
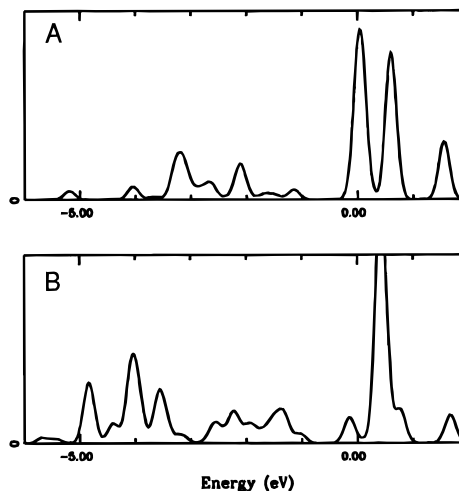

Figure 6. Projected CO $2\pi^*$-orbital density of states for the reactant state (A) and the transition state (B) of pathway b on the Cu_{10} cluster modeling the Cu(111) surface. The energies are with respect to the fermi level (E_f).

for both CO and NO are typically within 15 kcal/mol. For reaction paths c, the dissociation barriers for CO are 91, 88, and 85 kcal/mol for the 8-, 14-, and 28-atom clusters. The recombination barriers are 32, 20, and 31 kcal/mol, respectively, and the dissociation energies 58, 68, and 65 kcal/mol. However, the dissociated state for the first two clusters was not fully relaxed, so we should take into account the relaxation energy for the dissociated state on reaction path c of approximately 8 kcal/mol. Correcting for this, the barrier for recombination will increase by this amount, giving 40, 28, and 31 kcal/mol, and the dissociation energies will be lowered, resulting in the sequence 50, 60, and 65 kcal/mol. The differences between the 8- and 28-atom clusters are relatively large, but the values for the 14- and 28-atom clusters are within 5 kcal/mol. This is probably the upper limit for the error in the barrier on this pathway for clusters larger than 28 atoms. For NO, the differences in barriers and dissociation energies for the 14- and 28-atom clusters are somewhat larger (up to 14 kcal/mol); hence, the Cu_{14} clusters might be too small to model the NO dissociation on Cu(100). It is difficult to estimate the error due to the finite cluster size on Cu_{31}. From these results, we conclude that errors due to the finite cluster size can still be considerable. The trends are, therefore, the most meaningful results of this study, rather than the absolute energetics.

The activation barriers for dissociation for CO are significantly higher than those for NO, as expected because of the
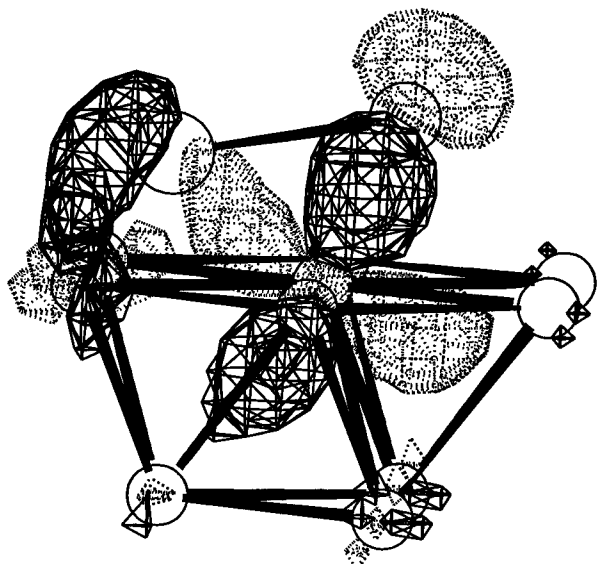
Figure 7. Bonding combination of CO $2\pi^*$ orbital and Cu(111) surface in the transition state for the top pathway (path b in Figure 1). The Cu_{10} framework is shown below, with seven atoms in the first layer and three atoms in the second layer. The carbon atom is located above the surface on the left side, and the oxygen atom is located on the right side. The density plot shows positive and negative values for the molecular wave function.

Figure 8. Schematic depiction of the influence of nonlocal corrections on reaction barriers and energetics. The dashed arrows show the energy change with respect to the local result. Indicated is the net effect on ΔH_{diss}, $\Delta E^{\ddagger}_{diss}$, and $\Delta E^{\ddagger}_{rec}$.

greater bond strength of CO compared to NO. It is consistent with Shustorovich's bond order conservation (BOC) concept, which relates energy barriers to, among others, the strength of the molecular bond that is being broken. The geometries also indicate a late transition state; the geometries of the transition states are closest to those of the dissociated states. In addition, the dissociation of CO and NO proceeds much easier on the more open Cu(100) surface than on the close-packed Cu(111) surface, in agreement with experiments that show a greater reactivity for more open surfaces toward NO dissociation.[16,17,50]

Another interesting conclusion can be made by comparing the bridged and diagonal reaction paths on either surface. On Cu(111), it is clearly the diagonal reaction path that is energetically favored for all systems studied, since we could rule out the bridged pathway that is too short for bringing about the dissociation. On Cu(100), however, the bridged pathway is indeed suitable to dissociate the diatomics, and it is, in fact, favored over the diagonal reaction pathway. This indicates that the two metal atoms are quite able to stabilize the transition state and, hence, lower the dissociation barrier. These findings are somewhat in contrast to earlier semiempirical calculations on CO dissociation on Rh. It would be interesting to extend the DFT calculations to these Rh systems.

Examining the adsorption and dissociation energies for the molecules, it is worth noting that for CO, the dissociation barriers are substantially higher than the adsorption energies (on average 90 vs 10 kcal/mol). Under moderate reaction conditions, CO will upon adsorption not be able to overcome the dissociation barrier. For NO, the dissociation barrier and adsorption energies are 40 and 20 kcal/mol, respectively. Hence, a thermally activated NO molecule could be able to overcome the dissociation barrier. These findings are in agreement with Cu single-crystal experiments where NO is observed to adsorb dissociatively while CO adsorbs molecularly.[21,23]

The nonlocal and local results show similar reactivity trends, although the absolute barriers and dissociation energy differ somewhat, as is explained in Figure 8. The correction for nonlocal effects appears to be largest for systems that have the strongest surface−adsorbate bonds. The dissociated state is
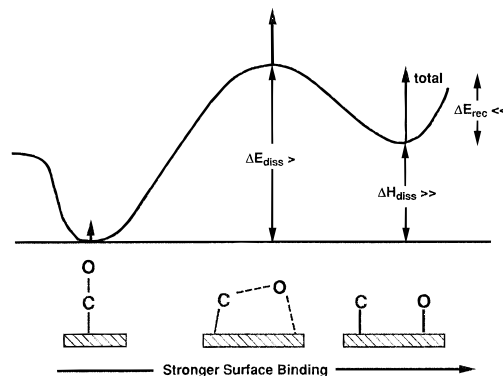
obviously stronger bonded than the reactant state since atom−surface bonds are generally stronger than molecule−surface bonds. The bond between the transition-state complex and the surface is likely of intermediate strength. If the correction for the transition state is larger than for the reactant state, it effectively increases the barrier for dissociation. We observed this for the majority of the systems that we studied (see Table 4). Since the DS is more corrected than the RS, the dissociation energy becomes more endothermic, and also, the barrier for recombination is lowered. An important conclusion is that it is justified to use the LDA approximation to predict trends in activation barriers. However, nonlocal corrections are essential to predict accurate reaction barriers and energies.

The mechanism for bond activation can be explained by analyzing the orbital interactions. For the Cu_{10} cluster, the fragment orbital density of states shows an increased importance of the contribution of the CO $2\pi^*$ to the adsorbate−surface interaction when the adsorbate tilts (Figure 6). For the linearly bound adsorbate, the $2\pi^*$ orbital mixes only to a small extent; most of the surface−adsorbate interaction is due to the CO 5σ orbital. However, when the adsorbate has tilted, there are many more possibilities for favorable overlap between the $2\pi^*$ orbital and surface orbitals, as is indicated by the increased density in the density of states spectrum. To illustrate this further, Figure 7 shows a bonding orbital that is constructed from the molecular $2\pi^*$ and a d orbital on the central Cu atom of the metal surface. This orbital is about 5 eV below the fermi level (E_f) and stabilizes the transition state. In addition, the $2\pi^*$−d interaction, although lowering the overall energy, results in a donation of electrons into the $2\pi^*$ orbital of the diatomic, hence destabilizing the molecular bond and facilitating the dissociation. This is the primary effect that explains the metal-activated bond breaking and can be expected to be applicable to many similar reactions on metal surfaces.

D. Normal Modes and Preexponential Factors. The vibrational frequencies of the adsorbates at the stationary points on the dissociation reaction pathways are reported in Tables 5 and 6. These were used to calculate the partition functions and the transition-state-theory preexponential factors. A frequency calculation is computationally more demanding than a geometry optimization since one can take less advantage of the symmetry of the system when doing finite displacements for all degrees of freedom. We therefore performed the frequency analysis mainly on the smallest clusters representing each reaction path (Cu_{10}, Cu_8, and Cu_{13}). A problem encountered when analyzing the normal modes for the diatomics and monoatomics on the surface was that the modes parallel to the surface are in some cases difficult to calculate. Unlike the stretching modes

NO and CO Dissociation on Cu(100) and Cu(111)

J. Phys. Chem., Vol. 100, No. 6, 1996 **2287**

TABLE 5: Vibrational Frequencies (cm^{-1}) and Partition Functions of CO at Stationary Points on the Reaction Paths

path	cluster	state	ν_1	ν_2	ν_3	ν_4	ν_5	$\nu6$	$Q_{\text{vib},T=300}$
b	Cu$_{19}$	RS	1802	315	205	202	57	54	60.6
	Cu$_{10}$	TS	565	495	425	353	i109	i388	2.5
	Cu$_{19}$	DS	534	375	375	502	360	360	2.5
c	Cu$_{21}$	RS	1564	214	388	388	102	102	14.6
	Cu$_8$	TS	570	520	474	353	227	i294	2.4
	Cu$_{21}$	DS	206	749	749	353	389	389	2.9
d	Cu$_{21}$	RS	1564	214	388	388	102	102	14.6
	Cu$_{13}$	TS	619	581	568	238	i135	i245	2.7
	Cu$_{21}$	DS	206	749	749	353	389	389	2.9

TABLE 6: Vibrational Frequencies (cm^{-1}) and Partition Functions of NO at Stationary Points, Analogous to Table 5

path	cluster	state	ν_1	ν_2	ν_3	ν_4	ν_5	ν_6	$Q_{\text{vib},T=300}$
b	Cu$_{19}$	RS	1481	214	263	236	90	90	26.1
	Cu$_{10}$	TS	564	501	497	357	i88	i427	2.4
	Cu$_{19}$	DS	537	425	425	502	360	360	2.3
c	Cu$_{21}$	RS	1280	252	470	470	116	116	9.8
	Cu$_8$	TS	529	478	380	250	230	i337	3.1
	Cu$_{21}$	DS	298	528	528	353	389	389	2.7
d	Cu$_{21}$	RS	1280	252	470	470	116	116	9.8
	Cu$_{13}$	TS	590	540	526	299	i112	i204	2.5
	Cu$_{21}$	DS	298	528	528	353	389	389	2.7

perpendicular to the surface, the bending modes appear to be more influenced by changes in the second nearest-neighbor shell of the adsorbate. Another difficulty is that the adsorption site does not have the same symmetry as the cluster. For instance, the reactant states for all reaction paths studied show a local C_{3v} or C_{4v} symmetry, whereas the whole cluster has only C_s symmetry. As a result, the adsorbate in a high-coordination adsorption site tends to move to the edge of the cluster, lowering its energy because of the coordinatively unsaturated edge atoms. This bending is an artifact of the cluster approach, and bending modes calculated for these distorted states cannot have great physical significance. To calculate accurate bending modes, we used larger clusters that have the same symmetry as the adsorption site as shown in Figure 9. We used a Cu$_{19}$ cluster to model the 3-fold site on a Cu(111) surface and a Cu$_{21}$ cluster to model the 4-fold site on a Cu(100) surface. The modes shown in Tables 5 and 6 for the reactant and product states result from these calculations. For the DS, we calculated the modes for each atom separately on the same clusters, hence neglecting the coupling between the atomic modes. This coupling is difficult to calculate since an atomic mode parallel to the surface can potentially mix in with modes of adsorbed species on all neighboring sites. Our results will, therefore, best describe the reactivity at low coverages. We did not find any experimental data on CO and NO adsorption in hollow sites, but the shift in stretch frequencies is realistic. The calculated internal CO stretching frequencies are in good agreement with the lowering of CO stretch frequencies observed for higher coordination numbers.[52] The Me—CO stretch is usually less dependent on the adsorption site, which makes it hard to draw conclusions for the calculated frequencies. A similar trend is found for the internal modes of chemisorbed NO. So *et al.*[14] reported NO-stretching frequencies of 1808 and 1520 cm^{-1} on Cu(111) for atop and 2-fold adsorbed NO, respectively. We calculated NO stretch frequencies for 3- and 4-fold sites of 1481 and 1280 cm^{-1}, respectively, in line with their experiments.

Experimental data on the parallel vibrational modes for diatomics on copper are unavailable. We therefore compared our calculated values to experimentally available equivalent modes on other metals, which we do not expect to be significantly different. Hindered translations for CO have been

Cu$_{19}$ (12, 7)   **Cu$_{21}$ (12, 9)**
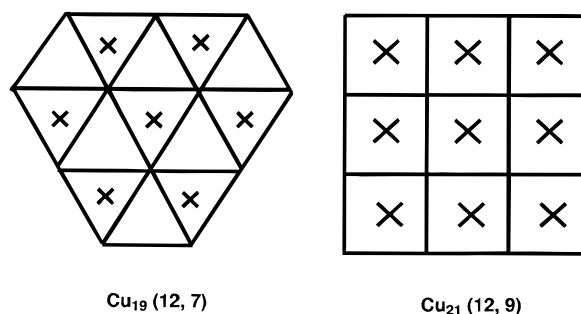
Figure 9. Cu$_{19}$ and Cu$_{21}$ clusters used to calculate the normal modes for diatomic and monoatomic adsorbates. Cluster representations as in Figure 1.

observed in the 25—100-cm^{-1} range on Pt(111) by Lahee *et al.*[55] They found a value of 71 cm^{-1} for top adsorbed CO and for 2-fold adsorbed CO values of 60 and 144 cm^{-1} (the degeneracy is lifted for the 2-fold site). Our values for NO and CO adsorbed in 4-fold hollow sites on Cu(100) are 100 and 116 cm^{-1}, respectively, in good agreement with their observations. Our values for CO adsorbed in a hollow site are 50 cm^{-1} on Cu(111) and 100 cm^{-1} on Cu(100). For NO, these values are 90 and 116 cm^{-1}, respectively, also in good agreement with their observations. The frequencies for hindered translations are expected to be lower on an open crystal surface than on a close-packed surface, since on an open surface it is possible to rotate a molecule through a larger angle before an interaction with the surrounding atoms starts to occur.[53] Our results agree with this. For 3-fold adsorbed CO and NO, we calculated a translational frequency of about half the frequency of the hindered translation for the 4-fold site. Hartree—Fock calculations show somewhat lower frequencies for CO on Cu(100), but this might be due to the lack of electron correlation in these methods.[54] For the hindered rotations, no experimental data are available, but they are expected to lie well above 150 cm^{-1},[55] in agreement with our findings.

For the vibrational frequencies of the atomic adsorbates, we were in some cases able to compare to experimental data. Sexton[56] measured a Cu(100)—O stretch between 290 and 330 cm^{-1} and Mohamed and Kesmodel[57] measured a Cu(100)—N stretch of 324 cm^{-1}. Typically our atom—surface stretch frequencies are within 50 cm^{-1} of the reported values.

For the transition states, the normal mode analysis for the Cu$_{10}$ and Cu$_{13}$ clusters yielded one more imaginary frequency besides the one corresponding to the reaction coordinate. This additional imaginary mode corresponds to the motion perpendicular to the symmetry plane, which implies that the calculated transition state is located on a maximum rather than a minimum for this degree of freedom. Any further optimization of the transition state moves CO/NO to the edge of the cluster due to the unsaturated edge atoms. This is an artifact due to cluster choice. To solve for this, the clusters have to be expanded to give a pure transition state. However, this requires a frequency calculation on a cluster of 31 metal atoms, which is not yet computationally feasible. We therefore estimated the asymmetric vibration with the value of the corresponding mode on the Cu$_8$ cluster (227 cm^{-1} for CO and 230 cm^{-1} for NO).

The computed preexponentials are given in Table 7. Preexponentials lower than 10^{13} s^{-1} relate to a decrease in entropy. This is the case going from reactant to transition state. The theoretically predicted preexponential factors correspond to tight transition states, with little rotational and translational motion. This result appears physically quite reasonable and results from the strong interaction of CO and NO in the transition state with the metal surface.

TABLE 7: Preexponential Factors (s^{-1}) for CO and NO Dissociation

	path	cluster	surface	k^0_{diss}	k^0_{rec}
CO	b	Cu$_{10}$	(111)	1.5×10^{11}	1.4×10^{13}
	c	Cu$_{8}$	(100)	1.0×10^{12}	1.3×10^{13}
	d	Cu$_{13}$	(100)	1.1×10^{12}	1.3×10^{13}
NO	b	Cu$_{10}$	(111)	3.4×10^{11}	1.6×10^{13}
	c	Cu$_{8}$	(100)	3.8×10^{12}	2.2×10^{13}
	d	Cu$_{13}$	(100)	2.0×10^{12}	1.1×10^{13}

Experimental results for the preexponential factors for dissociation show some variability but are generally well below the value of $k_B T/h$.[19] Astaldi *et al.*[58] reported experimental preexponentials for CO dissociation on Ni(100) of 5.4×10^9 and 1.2×10^{16} s^{-1} for recombination, showing similar changes in entropy going from reactants to products. Fink *et al.*[7] report preexponentials for NO dissociation on Pt(100) of 2.0×10^{15} s^{-1}. Lesley and Schmidt reported a preexponential for dissociation of NO on Pt(100) of 10^{13} s^{-1}, in good agreement with our values. Oh and co-workers[4] studied the reduction of NO by CO on single-crystal and polycrystalline Rh surfaces and found an activation barrier of about 20 kcal/mol for NO dissociation and measured a rate constant preexponential factor for NO dissociation of 6×10^{13} s^{-1}.

IV. Conclusions

We have performed density functional calculations on the dissociation of NO and CO on clusters simulating single-crystal surfaces of copper and calculated the energetics and the preexponential factors for the dissociation and recombination reaction. This serves as a model study for the conversion of NO and CO by exhaust catalysts. We have made a comparison of dissociation properties between NO and CO, between different reaction paths, and between the Cu(111) and Cu(100) surfaces.

The surfaces were represented by cluster models varying in size between 10 and 31 atoms. The barriers on the Cu(100) surface are significantly lower than on Cu(111) for both CO and NO. The activation barrier to dissociation appears to be correlated with the spacing between the nearest-neighbor sites. A large spacing results in low repulsion between the fragments after dissociation and a lower activation barrier for dissociation. A similar relation was found by Comrie *et al.* for NO dissociation on (111) surfaces of Pd, Pt, and Ni.[60] The dissociation barriers for NO on Cu(111) and Cu(100) were close to the NO adsorption energy. The barrier for CO dissociation, on the other hand, was at least 70 kcal/mol higher than its adsorption energy. This implies that NO can adsorb dissociatively on Cu(111) and Cu(100) surfaces, but CO will adsorb molecularly. This agrees with experiments that observe dissociative adsorption of NO at Cu, even at low temperatures, but no dissociation for CO.[16] Applying nonlocal corrections does not alter the trends that we found using a local potential. However, the absolute values for especially the recombination barriers and the reaction enthalpy are affected considerably by introducing nonlocal corrections.

The effect of cluster size on the energetics that we described is still considerable. However, we found reliable trends even with relatively small clusters (13−14 atoms). The use of clusters with more than 20 atoms solved some of the problems that are related with clusters of smaller size, the main problem being the coordinative unsaturation of cluster atoms that are directly neighboring the adsorbate.

We used transition-state theory to calculate the preexponentials for dissociation. The normal modes were calculated for the reactant, transition, and product states to obtain the vibrational partition functions. It turned out to be important to increase the cluster size for calculating the normal modes parallel to the surface for the adsorbed species. We used clusters of 19 and 21 atoms to get reliable values for these modes. The entropy factor appears to be more important for NO than for CO dissociation. The calculated preexponentials correspond to a tight transition state for dissociation.

References and Notes

(1) Nieuwenhuys, B. E. *Surf. Sci.* **1983**, *126*, 307.
(2) Taylor, K. C. *Automobile Catalytic Converters*; Springer: Berlin, 1988.
(3) Root, T. W.; Schmidt, L. D.; Fisher, G. B. *Surf. Sci.* **1983**, *134*, 30.
(4) Oh, S. H.; Fisher, G. B.; Carpenter, J. E.; Goodman, D. W. *J. Catal.* **1986**, *100*, 360.
(5) Shelef, M.; Graham, G. W. *Catal. Rev., Sci. Eng.* **1994**, *36*, 433.
(6) Banse, B. A.; Wickham, D. T.; Koel, B. E. *J. Catal.* **1989**, *119*, 238.
(7) Fink, Th.; Dath, J.-P.; Basset, M. R.; Imbihl, R.; Ertl, G. *Surf. Sci.* **1991**, *245*, 96.
(8) Biloen, P.; Sachtler, W. H. H. *Adv. Catal.* **1981**, *30*, 165.
(9) A recent discussion can be found in: *Applied Catalysis B: Environmental, 2*; Elsevier: Amsterdam, 1993.
(10) Ziegler, T. *Organometallics* **1994**, *13*, 2252.
(11) Van Daelen, M. A.; Newsam, J. M.; Van Santen, R. A. To be published.
(12) Tracy, J. C. *J. Chem. Phys.* **1972**, *56*, 2748.
(13) Hollins, P.; Pritchard, J. *Surf. Sci.* **1979**, *89*, 486.
(14) So, S. K.; Franchy, R.; Ho, W. *J. Chem. Phys.* **1991**, *95*, 1385.
(15) Wendelken, J. F. *J. Vac. Sci. Technol.* **1982**, *20*, 884.
(16) Balkenende, A. R.; Gijzeman, A. L. J.; Geus, J. W. *Appl. Surf. Sci.* **1989**, *37*, 189.
(17) Balkenende, A. R.; Den Daas, H.; Huisman, M.; Gijzeman, A. L. J.; Geus, J. W. *Appl. Surf. Sci.* **1991**, *47*, 341.
(18) Brodén, G.; Rhodin, T. N.; Brucker, C.; Benbow, R.; Hurych, Z. *Surf. Sci.* **1976**, *59*, 593.
(19) Campbell, C. T.; Sun, Y. K.; Weinberg, W. H. *Chem. Phys. Lett.* **1991**, *179*, 53.
(20) Post, D.; Baerends, E. J. *J. Chem. Phys.* **1983**, *78*, 5663.
(21) Te Velde, G.; Baerends, E. J. *Chem. Phys.* **1993**, *177*, 399.
(22) Bauschlicher, C. W. *J. Chem. Phys.* **1994**, *101*, 3250.
(23) Philipsen, P. H. T.; Te Velde, G.; Baerends, E. J. *Chem. Phys. Lett.* **1994**, *226*, 583.
(24) Harris, J.; Andersson, S. *Phys. Rev. Lett.* **1985**, *55*, 1583.
(25) Feibelman, P. J. *Phys. Rev. Lett.* **1991**, *67*, 461.
(26) Yang, H. Y.; Whitten, J. *J. Chem. Phys.* **1993**, *98*, 5039.
(27) De Koster, A.; Van Santen, R. A. *Surf. Sci.* **1990**, *233*, 366.
(28) Shustorovich, E. *Adv. Catal.* **1990**, *37*, 101.
(29) Van Langeveld, A. D.; De Koster, A.; Van Santen, R. A. *Surf. Sci.* **1990**, *255*, 143.
(30) Nygren, M. A.; Siegbahn, P. E. M. *J. Phys. Chem.* **1992**, *96*, 7579.
(31) Siegbahn, P. E. M. *Surf. Sci.* **1992**, *269*, 276.
(32) Burghgraef, H.; Jansen, A. P. J.; Van Santen, R. A. *J. Chem. Phys.* **1993**, *98*, 8810.
(33) Burghgraef, H.; Jansen, A. P. J.; Van Santen, R. A. *Chem. Phys.* **1993**, *177*, 407.
(34) Burghgraef, H.; Jansen, A. P. J.; Van Santen, R. A. *J. Chem. Phys.* **1994**, *101*, 11012.
(35) Blaskowski, S.; Jansen, A. P. J.; Nascimento, M. A. C.; Van Santen, R. A. *J. Phys. Chem.* **1994**, *98*, 12938.
(36) Van Daelen, M. A.; Li, Y. S.; Newsam, J. M.; Van Santen, R. A. *Chem. Phys. Lett.* **1994**, *226*, 100.
(37) Delley, B. *J. Chem. Phys.* **1990**, *92*, 508.
(38) Baerends, E. J.; Ellis, D. E.; Ros, P. *Chem. Phys.* **1973**, *2*, 41.
(39) Von Barth, U.; Hedin, L. *J. Phys. C* **1972**, *5*, 1629.
(40) Ceperley, D. M.; Alder, B. J. *Phys. Rev. Lett.* **1980**, *45*, 566.
(41) Becke, A. D. *Phys. Rev. A* **1988**, *38*, 3098.
(42) Perdew, J. P. *Phys. Rev. B* **1986**, *33*, 8822.
(43) Lind, D. M.; Dunning, F. B.; Walters, G. K.; Davis, H. L. *Phys. Rev. B* **1987**, *35*, 9037.
(44) Lindgren, S. A.; Wolldin, L.; Rundgren, J.; Westrin, P. *Phys. Rev. B* **1984**, *29*, 576.

NO and CO Dissociation on Cu(100) and Cu(111)

J. Phys. Chem., Vol. 100, No. 6, 1996 **2289**

(45) Baker, J. *J. Comp. Chem*. **1986**, *7*, 385.

(46) Laidler, K. J. *Chemical Kinetics*, 3rd ed.; Harper and Row: New York, 1987.

(47) Glasstone, S.; Laidler, K. J.; Eyring, H. *The theory of rate processes*; McGraw-Hill: New York, 1941.

(48) Huber, K. P.; Herzberg, G. *Molecular Spectra and Molecular Structure*; Van Nostrand-Reinhold: New York, 1979; Vol. IV.

(49) Van Santen, R. A.; Zonnevylle, M.; Jansen, A. P. J. *Phil. Trans. R. Soc. London, Ser. A* **1992**, *341*, 269.

(50) Johnson, D. W.; Matloob, M. H.; Roberts, M. W. *J. Chem. Soc., Faraday Trans. 1* **1979**, *75*, 2143.

(51) Benzinger, J. B.; Preston, R. E. *Surf. Sci*. **1984**, *141*, 567.

(52) Sheppard, N.; Nguyen, T. T. In *Advances in Infrared and Raman Spectroscopy*; Clark, R. J. H., Hester, R. E., Eds.; Heyden: London, 1978; Vol. 5.

(53) Schweizer, E.; Persson, B. N. J.; Tüshaus, M.; Hoge, D.; Bradshaw, A. M. *Surf. Sci*. **1989**, *213*, 49.

(54) Head-Gordon, M.; Tully, J. *Chem. Phys*. **1993**, *175*, 37. Tully, J. Personal communications.

(55) Lahee, A. M.; Toennies, J. P.; Wöll, Ch. *Surf. Sci*. **1986**, *177*, 371.

(56) Sexton, B. A. *Surf. Sci*. **1979**, *88*, 299.

(57) Mohamed, M. H.; Kesmodel, L. L. *Surf. Sci*. **1987**, *185*, L467.

(58) Astaldi, C.; Santoni, A.; Della Valle, F.; Rosei, R. *Surf. Sci*. **1989**, *220*, 322.

(59) Lesley, M. W.; Schmidt, L. D. *Surf. Sci*. **1985**, *155*, 215.

(60) Comrie, C. M.; Weinberg, W. H.; Lambert, R. M. *Surf. Sci*. **1976**, *57*, 619.

(61) Andersson, S.; Pendry, B. N. J. *Phys. Rev. Lett*. **1979**, *43*, 363.

(62) Andersson, S. *Surf. Sci*. **1979**, *89*, 477.